J Mater Sci: Mater Electron (2015) 26:4290–4297
DOI 10.1007/s10854-015-2981-8

CrossMark

Ultraviolet nano-photodetector based on ZnS:Cl nanoribbon/Au Schottky junctions

Li Wang[1,2] · Xu Ma[1] · Ran Chen[1] · Yong-Qiang Yu[1] · Lin-Bao Luo[1]

Received: 19 January 2015 / Accepted: 19 March 2015 / Published online: 17 April 2015
© Springer Science+Business Media New York 2015

Abstract We report on a semiconductor nanostructures/metal Schottky junction for optoelectronic device application. The *n*-type ZnS nanoribbons (NRs) with an electron mobility of 64.9 cm V^{-1} s^{-1} and electron concentration of 5.7×10^{17} cm^{-3} were synthesized by using Cl as dopant via a thermal co-evaporation method. Electrical analysis reveals that the Schottky barrier diodes (SBD) based on the ZnS:Cl NRs/Au junctions exhibited typical rectifying behavior (rectification ratio $>10^3$) with Schottky barrier height of .64 eV and a small ideality factor of $\sim$1.05 at 320 K. Interestingly, *n*-ZnS:Cl NR/Au nano-SBD device exhibited pronounced negative photoresponse at forward bias, but positive photoresponse at reverse bias under 365 nm UV light irradiation. Finally, the detailed reason for this phenomenon was explained by the energy band diagram.

1 Introduction

One-dimensional (1-D) II–VI group semiconductor materials (e.g. CdS, CdSe, CdTe, ZnS, ZnSe, ZnTe, etc.) have been attracting extensive research attention lately due to their promising potential in future nano-electronic and nano-optoelectronic systems. [1–4] Among the various II–VI group semiconductors, zinc sulfide (ZnS) with a direct band-gap of 3.70 eV and a large exaction binding energy of 40 meV at room temperature is of particular interest. [5, 6] Up to now, various 1-D ZnS nanostructures including nanowire (NWs), nanoribbons (NRs), nanobelts (NBs) have been successfully synthesized by various methods [7, 8] Like other semiconductors, when the size and dimensional shrink to the nanoscale level, 1-D ZnS nanostructures are expected to exhibit a quantum-size effect which might bring out improved physical, catalytical and optical properties and therefore induce new applications in photonic devices.

Due to the distinct characteristics such as wide band gap in the UV regime, high crystallinity, as well as high quantum efficiency, ZnS nanostructures have demonstrated marvelous versatility and have been regarded as one of the most promising materials for optoelectronic devices application, [9, 10], including light-emitting diodes (LEDs), [11], solar cell [12], injection lasers, [13], field effect transistors (FETs), [14, 15], and so on. Another important application of ZnS nanostructures is for efficient ultraviolet photodetectors (UVPDs), [16, 17], which are vitally important for flame sensing, space communication, ozone-layer monitoring, and so on. Owing to the distinct absorption characteristics and appropriate band gap (3.77 eV for the hexagonal wurtzite phase and 3.72 eV for the cubic phase), 1-D ZnS nanostructures are suitable for UV sensing against a background with infrared and visible irradiation. To date, while several photoconductive-type ultraviolet photodetectors solely based on ZnS nanostructures have been reported, relatively little attention has been paid to UV photodetector based on metal/ZnS nanostructures Schottky junction, which have obvious advantages in high

✉ Li Wang
wlhgd@hfut.edu.cn

✉ Yong-Qiang Yu
yongqiangyu@hfut.edu.cn

✉ Lin-Bao Luo
luolb@hfut.edu.cn

[1] School of Electronic Sciences and Applied Physics and Anhui Provincial Key Laboratory of Advanced Materials and Devices, Hefei University of Technology, Hefei 230009, Anhui, People's Republic of China

[2] Department of Materials Science and Engineering, University of Toronto, Toronto, ON M5S 3E4, Canada

sensitivity, fast response speed and low energy consumption over traditional photoconductive type UVPDs [18–20].

Intrinsic II–VI group nanostructures are usually not suitable for device applications as it is virtually electrically insulative without doping. Thus doping is vitally important for II–VI semiconductor nanostructrues for the feasibility to tune the electronic as well as optoelectronic properties in a wide range [21, 22]. Chloride (Cl) has proven to be an efficient dopant to achieve high quality *n*-type ZnS material [9, 23]. And our previous study showed that the ZnS nanoribbons doped with Cl element exhibit excellent optoelectronic properties [24]. In this work, we present a simple UV light nano-photodetector based on Au/chlorine doped ZnS NR Schottky junction. The *n*-type ZnS:Cl NRs with carrier mobility and concentration were 64.9 cm^2 V^{-1} S^{-1} and 5.7×10^{17} cm^{-3}, respectively were synthesized by using $ZnCl_2$ as dopant via a thermal co-evaporation method. Electrical analysis reveals that the ZnS:Cl NRs/Au Schottky junction diode exhibited obvious rectifying behaviors (rectification ratio $>10^3$) with Schottky barrier height of .64 eV and a ideality factor of ~ 1.05 at 320 K. In addition, under UV light irradiation, the nano-SBD device exhibit obvious negative photoresponse at forward bias, but positive photoresponse at negative bias. Detailed reason for this phenomenon was clarified by the energy band diagram at last.

2 Experimental section

2.1 Synthesis and characterization of ZnS:Cl NRs

The ZnS:Cl NRs were synthesized in a horizontal quartz tube furnace (inner diameter 30 mm, length 120 cm) via a thermal co-evaporation method. Briefly, ZnS power (99.99 %, Aldrich) was first loaded into an alumina boat which was placed to the center region of the furnace. Another boat containing $ZnCl_2$ powder was used as the Cl dopant source and placed at downstream, about distance of 12 cm upstream from ZnS source. Si substrates coated with 5 nm gold were placed at the downstream direction, $\sim$10 cm from the ZnS source. The molar ratio of $ZnCl_2$:ZnS was kept at 1:2 [24]. The system was then evacuated to a base pressure of 4×10^{-5} Torr, and then backfilled with a mixture gas of 40 standard-state cubic centimeter per minute (sccm) Ar and H_2 (5 % in volume). The ZnS source was heated up to 1060 °C and maintained at this temperature for 90 min. The morphologies and structures of the as-synthesized ZnS:Cl NRs were characterized by X-ray diffraction (D-500 using Cu Kα radiation), field-emission scanning electron microscopy (FE-SEM, SIRION 200 FEG) and high-resolution transmission electron microscopy (HRTEM, Philips CM200 FEG). The chemical compositions of the ZnS:Cl NRs were analyzed by X-ray photoelectron spectroscopy (XPS, Thermo ESCALAB 250).

2.2 Construction and characterization of FETs and SBDs based on individual Cl doped ZnS NRs

To study the electrical property of the ZnS:Cl NRs, FETs based on individual ZnS NR were constructed. Briefly, ZnS NRs were first dispersed on the SiO_2 (300 nm)/p^+-Si substrate with desired density. Afterwards, ITO source and drain electrodes were defined by shadow mask and pulsed laser deposition (PLD) system with KrFexcimer laser (Lambda PhysikCOMPexPro102, 248 nm, 120 mJ, 5 Hz). In this method, the shadow mask was made by etching 25 μm thick copper foils. To assemble a nano-SBD device, additional photolithography and lift-off process were performed to define the Au (80 nm) electrode. All the electrical measurements were carried on a semiconductor *I-V* characterization system (Keithley 4200-SCS). The temperature-dependent electrical measurements were performed using a low-temperature system (Janis/CCS-350S). To detect the photoconductive properties of ZnS:Cl NR, monochromatic light from a 100 W monochromator (Omni-λ365) was focused and guided perpendicularly onto the NRs. The light was turned on and off manually to study the time response of the ZnS:Cl NR/Au SBDs UV PD.

3 Results and discussions

Figure 1a shows a typical SEM image of the as-obtained nanostructures, from which one can see that the product is mainly composed of fiber-like geometry. Further image at large magnification shows that the nanostructures are 1–2 μm in width, 20–100 μm in length, and 30–50 nm in thickness. Figure 1d shows a typical HRTEM image and corresponding selected area electron diffraction (SAED) pattern, revealing that the NRs have a single-crystal zinc blende structure with a growth orientation of [002]. The XRD diffraction peaks can be assigned to wurtzite ZnS (JCPDS no.80-0007) with no impurity phases (Fig. 1b), [25, 26] suggesting the high phase purity of the product. Figure 1f depicts the energy-dispersive X-ray (EDX) spectroscopy profile of the NR, according to which, the atomic ratio of Zn/S is estimated to be 50:49, in agreement with the stoichiometric ratio of ZnS NRs. Due to low doping concentration, the doped Cl atoms cannot be detected by the EDX analysis. However, its presence can be easily confirmed by XPS investigation. Figure 2a display the XPS survey spectrum of the Cl doped ZnS NRs, it can be seen that, in addition to the signal due to Zn and S, there

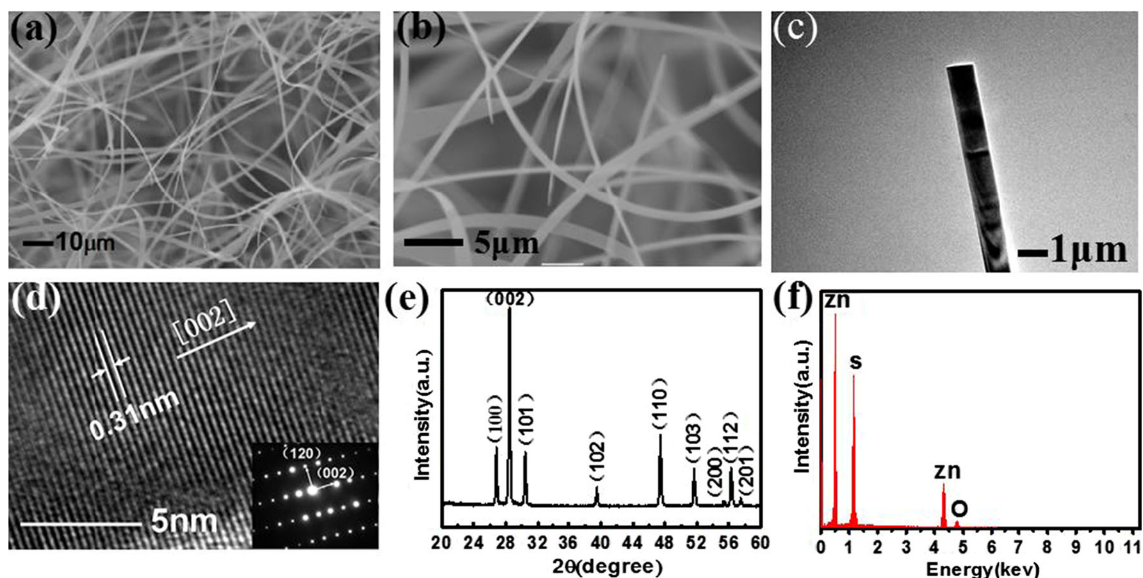

Fig. 1 **a** A typical SEM image of ZnS:Cl NRs. **b** SEM image of ZnS:Cl NRs at large magnification. **c** TEM image of a typical ZnS NR. **d** HRTEM image of the ZnS:Cl NR, the inset shows the corresponding SAED pattern. **e** XRD pattern of Cl-doped ZnS NRs. **f** The EDX spectrum

Fig. 2 **a** XPS survey spectrum of the ZnS:Cl NRs. **b**, **c** Shows the enlarged Cls and Cl2p peaks, respectively

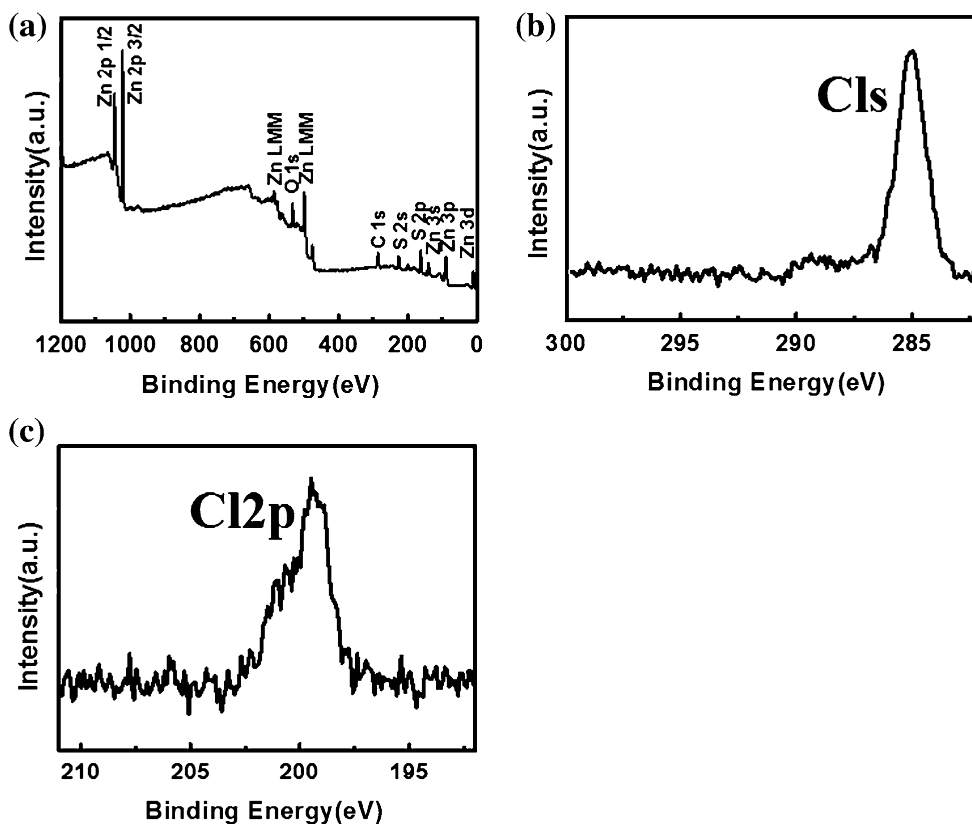

are two peaks locating at 284 and 199 eV, ascribable to the binding energy of Cl s and Cl 2p, respectively.

FETs based on individual ZnS:Cl NRs were constructed to investigate the electrical properties of ZnS:Cl NRs. In this study, we used indium doped tin dioxide (ITO) as electrode material, and we found that the deposition method is the key to form good contact to the NR. Figure 3a compares the *I*-*V* curves of the ZnS:Cl NR with ITO electrode shape defined by lithography and shadow mask respectively. Obviously, when the shape of ITO electrode

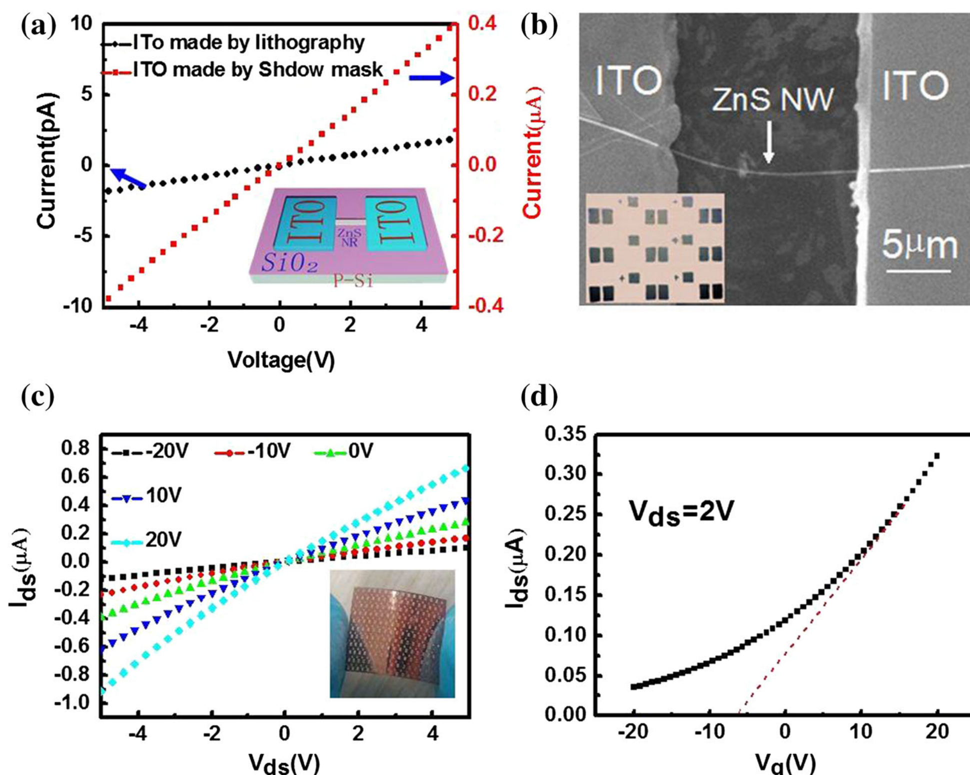

Fig. 3 **a** The *I-V* curve of the ZnS:Cl NR/ITO electrode, which was defined by either lithography or shadow mask. **b** Representative SEM image of a single NR device fabricated by shadow mask, the inset shows the photograph of the device. **c** I_{ds}–V_{dS} curves at varied V_g. **d** I_{ds}–V_g curves at $V_{ds} = 2$ V

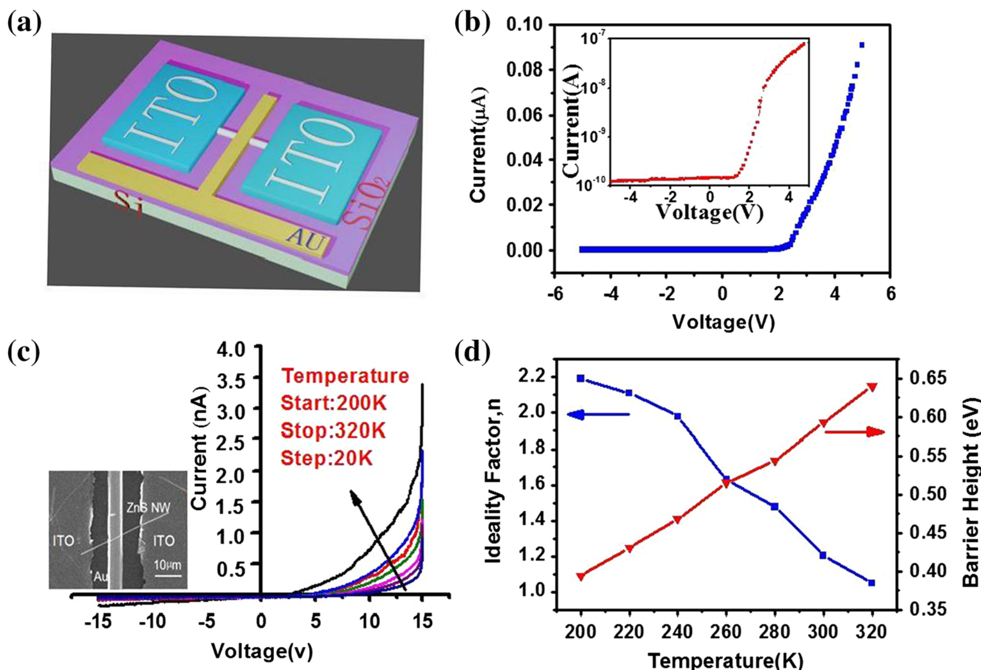

Fig. 4 **a** Schematic illustration of the nano-SBD device. **b** Room-temperature rectifying characteristics of the nano-SBD, the *inset* shows the semi-logarithmic plot of the rectifying curve. **c** Rectifying characteristics of the nano-SBD measured at varied temperatures from 200 to 320 K, the *inset* shows a typical SEM image of the nano-SBD fabricated from a single ZnS:Cl NR. **d** Temperature dependence of the ideality factor and the barrier height of the nano-SBD

was defined by photolithography, followed ITO deposition through PLD, the current of ZnS:Cl NR is virtually insulating (the value is on the order of 10^{-12} A). Nonetheless, the current is as high as $\sim 10^{-6}$ A, if the ITO electrode was directly deposited by a copper mask shadow assisted PLD. According to previous study, a highly conductive interface is probably between ZnS and ITO during PLD process. In this process, the surface of ZnS was oxidized and some indium atoms would diffuse into the oxidation layer, promoting the injection of electrons into the ZnS nanoribbons via direct tunneling [24]. The formation of high-conductivity interfacial oxide layer can be easily realized when the

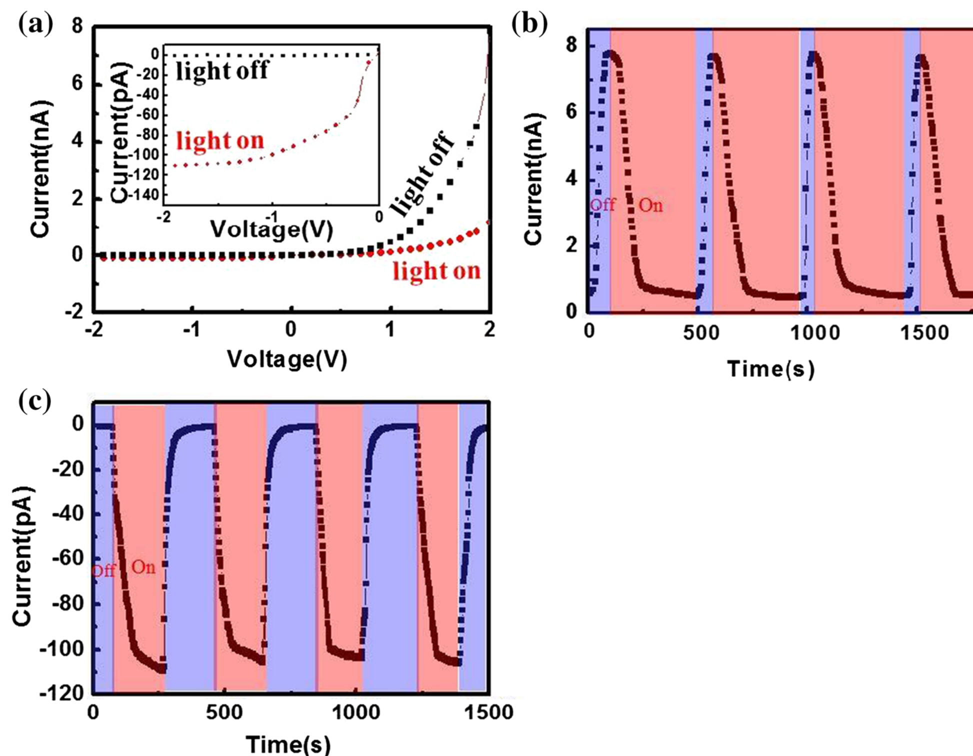

Fig. 5 **a** *I–V* curve of the *n*-ZnS NR/Au Schottky diode in dark and under UV light. The photoresponse of the *n*-ZnS NR/Au Schottky diode and forward bias of 2 V (**b**), at reverse bias of 2 V (**c**). The wavelength of the light is 365 nm, what is more, the light intensity is 100 μ W cm^{-2}

Table 1 Summary of device performance of similar semiconductors nanostructures based photodetectors

Structures	Device	R (AW^{-1})	G	I_{light}/I_{dark}	References
Au/ZnS:Cl NR (Reverse bias)	Schottky junction	9.1	33	180	This work
Graphene/ZnONR array	Schottky junction	113	385	~85	[35]
Au/SiO_2/ZnONR array	Schottky junction	100–1000	337	/	[36]
ZnONW/Si-MgO/n-Si	n-i-n junction	/	/	~8000	[37]
GaN/Ag	Schottky junction	4.2	14.2	~100	[38]
Graphene oxide and carbon nanotube film/n-ZnO NRs	p-n junction	2.4	8.1	~1.2	[39]

ITO electrode is directly deposited by mask shadow assisted PLD. Unfortunately, once the ITO electrode was defined by photolithography, followed by PLD deposition. The aqueous solution as well as residual photoresist will destroy the formation of highly conductive interface. In light of the above, the ITO electrodes were fabricated by PLD system with the aid of Cu shadow mask. Figure 3b shows a representative SEM image of a single NR device, in which the ITO was deposited by PLD with the assistance of shadow mask (the inset shows a typical photograph). It was clear that accurate contact shape can be obtained with copper mask, which is very important for further device construction. Figure 3c plots the typical gate-dependent source-drain current (I_{ds}) versus source-drain voltage (V_{ds}) curves of ZnS:Cl NR at varied V_g from −20 to 20 V at a step of 10 V. Obviously, the I_{ds} decreases with decreasing gate voltage, suggesting *n*-type conducting channel of the ZnS:Cl NR FET. The electron mobility μ_n can be further determined to be 64.9 cm V^{-2} s^{-1}, according to the following equations: $g_m = \partial I_{DS}/\partial V_G = Z\mu_n C_0 V_{Ds}/L$, where Z/L (1/15 μm) is the width-to-length ratio of the NR channel [27, 28], C_0 the oxide capacitance per unit area, g_m the transconductance of the nano-FET, which can be deduced to ~59.7 nS in the linear regime of I_{ds}–V_g curve by the relationship of $g_m = dI_{ds}/dV_g$ (Fig. 3d). What is more, the electron concentration n_e can be estimated to be 5.7×10^{17} cm^{-3} by the formula of $n_e = 1/\rho q \mu_e$, where ρ is the resistivity of the NR, q is the elementary charge (1.6×10^{-19} C).

Next, *n*-ZnS NR/Au nano-SBDs were constructed to explore the potential applications of the *n*-type ZnS NRs in nanoelectronic devices. Figure 4a, c show the schematic

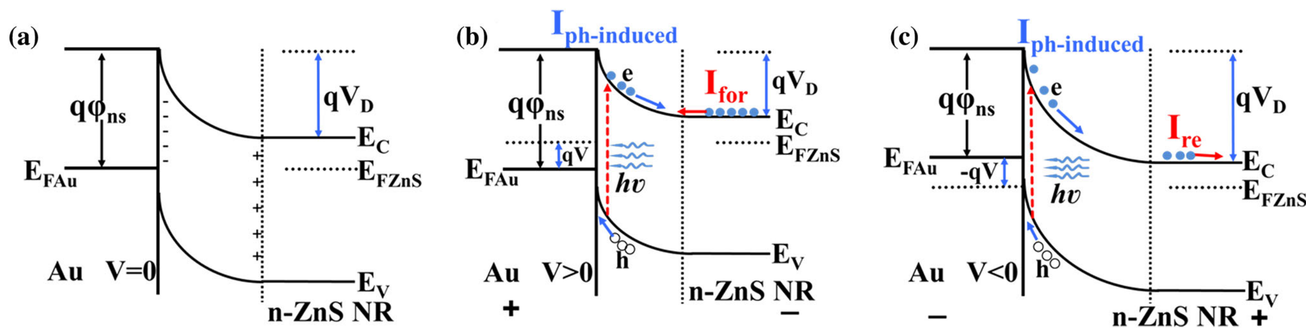

Fig. 6 Energy band diagram of the *n*-ZnS NR/Au SBD UVPDs upon light illumination without bias voltage (**a**), with forward bias voltage (**b**), with reverse bias voltage (**c**)

illustration and a typical SEM image of the device, respectively. From the room-temperature *I–V* characteristics in Fig. 4b, one can see that the device show typical rectification behavior, with a high rectification ratio of $>10^3$ and a turn-on voltage of $\sim$2.0 V. What is more, no obvious reverse-bias breakdown is observed up to -5 V, suggesting the good quality of the *n*-ZnS NR/Au Schottky junction. Figure 4c depicts the temperature dependent rectifying characteristics of the nanoSBD, as the temperature increases from 200 to 320 K, the turn-on voltage shifts from 8.40 to 2.0 V, along with an increase of forward current. According to previous study, the conduction current of SBD is usually composed of thermionic emission current and tunneling current. Assuming that the thermionic emission is the most predominant mechanism [29, 30], the rectifying characteristics of the nano-SBD can be described by the following equations [31, 32]: $I = I_0\left[\exp(qV/nkT) - 1\right] \approx I_0 \exp(qV/nkT)$ and $I_0 = AA{*}\,T^2\ \exp(-q\Phi_b/kT)$, where I_0 is the reverse saturation current, n is the ideality factor, A is the area of Schottky contact, Φ_b is the Schottky barrier height, and A^* is the effective Richardson constant (80.0 Acm^{-2} K^{-2} for ZnS). Figure 4d plots the relationship of n and Φ_b with temperature. It is found that when the temperature increases from 200 to 320 K, n will decrease from 2.19 to 1.05, meanwhile, the Φ_b will increase from .39 to 0.64 eV. Although this temperature-dependent Schottky barrier height is different from the conventional Schottky theory (Φ_b normally decreases with increasing temperature), similar phenomena have been observed on Au/n-Si Schottky barrier diode, [33] in which electrons possessing a weak kinetic energy at low temperatures prefer to pass through a low barrier, thus leading to a lower barrier height and larger ideality factor at low temperatures.

Interestingly, the *n*-ZnS:Cl NR/Au nano-SBD device exhibited pronounced negative photoresponse at forward bias, but positive photoresponse at reverse bias under UV light irradiation (the wavelength is 365 nm). As observed in Fig. 5c, the electrical current at reverse bias increased dramatically and stabilized at a high-conduction “on” state upon light radiation, but it decreased quickly to a low-conductivity “off” state after the UV light was turned off, in contrast to the case at forward bias (Fig. 5b). To evaluate the device performance of such *n*-ZnS NR/Au nano-SBD device in a quantitative way, we then calculated the key parameters including responsivity (R), photoconductive gain (G). The R can be expressed by the formula of $R(AW^{-1}) = I_p/P_{opt} = \eta(q\lambda/hc)G$, [34] where I_p, P_{opt}, η, λ, h, c and G are the photocurrent, the incident light power, the quantum efficiency, the light wavelength, the Planck’s constant, the light speed and the photoconductive gain, respectively. Based on the above equation, by assuming $\eta = 1$ for simplification, R is estimated to be 9.1AW^{-1} for the nano-SBDs. Meanwhile, G is calculated to be 33, in comparison with other UV PDs with similar device configuration (Table 1).

To interpret the different photoresponse characteristics of the Au/ZnS:Cl NR Schottky junction at both forward and negative bias voltage, the energy band diagram of the diode at different biases were illustrated in Fig. 6. It is obvious that when no bias is applied (Fig. 6a), the band of the *n*-ZnS NR near the metal/semiconductor interface bent upwards with barrier height qV_D, forming a space-charge region. At the forward bias (Fig. 6b), the barrier height (qV_D) was reduced and the diodes is turned on, allowing the electrons in the *n*-ZnS NR pass through the Schottky barrier and reach the Au electrode, forming a current called $I_{forward}$. Upon light illumination, electron–hole pairs will be generated in ZnS NR near the junction, and separated due to the built-in electric field, leading to a photocurrent ($I_{photo\text{-}induced}$) with an opposite direction compared to that of the Schottky diode at the forward bias, as demonstrated in Fig. 6b. Thereby, the photocurrent (I_{light}) is believed to the sum of such two currents with opposite direction as mentioned above, resulting in a reduction in photocurrent and interesting negative photoresponse at forward bias.

Similar negative photoconductivity phenomena can be found in previous studies on semiconducting nano-Schottky barrier diode photodetectors and other devices based on surface dominated materials. [40–43] As for the positive photoresponse at reverse bias, it should be associated with two overlapping current with the same direction, as demonstrated in Fig. 6c [44].

4 Conclusions

In summary, a simple UV light nano-photodetector was fabricated by using *n*-type chlorine doped ZnS NRs as building blocks, which were synthesized by using Cl as dopant. Electrical analysis reveals that the electron mobility and concentration were 64.9 $cm^2 V^{-1} S^{-1}$ and 5.7×10^{17} cm^{-3}, respectively. It is also found that the ZnS:Cl NRs/Au Schottky junction diode exhibited remarkable rectifying behaviors (rectification ratio $>10^3$) with Schottky barrier height of .64 eV and a small ideality factor of $\sim$1.05 at 320 K. What is more, when irradiated by UV light illumination, the nano-SBDs show negative photoresponse at forward bias, but positive photoresponse at reverse bias, with good reproducibility. The detailed reason for this phenomenon was explained by the energy band diagram at last.

Acknowledgments This work was supported by the financial supports from the China Scholarship Council, the Natural Science Foundation of China (Nos. 61106010, 21101051), the Natural Science Foundation of Anhui Province (J2014AKZR0059), and the Fundamental Research Funds for the Central Universities (Nos. 2013HGXJ0195, 2012HGCX0003, 2013HGCH0012, 2014HGCH0005).

References

1. J.S. Jie, W.J. Zhang, I. Bello, C.S. Lee, S.T. Lee, One-dimensional II–VI nanostructures: synthesis, properties and optoelectronic applications. Nano Today **5**, 313–336 (2010)
2. S.K.J. Al-Ani, R.A. Ismail, H.F.A. Al-Ta'ay, Optoelectronic properties n: CdS:In/p-Si heterojunction photodetector. J. Mater. Sci. Mater. **E117**, 819–824 (2006)
3. J.A. Zapien, Y. Jiang, X.M. Meng, W. Chen, F.C.K. Au, Y. Lifshitz, S.T. Lee, Room-temperature single nanoribbons lasers. Appl. Phys. Lett. **84**, 1189–1191 (2004)
4. L.B. Luo, X.L. Huang, M.Z. Wang, C. Xie, C.Y. Wu, J.G. Hu, L. Wang, J.A. Huang, The effect of plasmonic nanoparticles on the optoelectronic characteristics of CdTe nanowires. Small **10**, 2645–2652 (2014)
5. X.S. Fang, Y. Bando, G.Z. Shen, C.H. Ye, U.K. Gautam, P.M.F.J. Costa, C.Y. Zhi, C.C. Tang, D. Golberg, Ultrafine ZnS nanobelts as field emitters. Adv. Mater. **19**, 2593–2596 (2007)
6. N. Hebalkar, A. Lobo, S.R. Sainkar, S.D. Pradhan, W. Vogel, J. Urban, S.K. Kulkarni, Properties of zinc sulphide nanoparticles stabilized in silica. J. Mater. Sci. **36**, 4377–4384 (2001)
7. G.Z. Shen, B. Liang, X.F. Wang, H.T. Huang, D. Chen, Z.L. Wang, Ultrathin In_2O_3 nanowires with diameters below 4 nm: synthesis, reversible wettability switching behavior, and transparent thin-film transistor applications. ACS Nano **5**, 6148–6155 (2011)
8. B. Nie, L.B. Luo, J.J. Chen, J.G. Hu, C.Y. Wu, L. Wang, Y.Q. Yu, Z.F. Zhu, J.S. Jie, Fabrication of p-type nanowires for high-performance ultraviolet light photodetector application. Nanotechnology **24**, 096503 (2013)
9. A. Kato, M. Katayama, A. Mizutani, Y. Hattori, N. Ito, T. Hattori, Satellite peak generation in the electroluminescence spectrum of ZnS:Sm grown by metalorganic chemical vapor deposition with Clcodoping. J. Appl. Phys. **76**, 3206–3208 (1994)
10. E. Bacaksiz, O. Gorur, A. Tomakin, E. Yanmaz, A. Altunbas, Ag diffusion in ZnS thin films prepared by spray pyrolysis. Mater. Lett. **61**, 5239–5242 (2007)
11. L.D. Sun, C.H. Liu, C.S. Liao, C.H. Yan, ZnS nanoparticles doped with Cu(I) by controlling coordination and precipitation in aqueous solution. J. Mater. Chem. **9**, 1655–1657 (1999)
12. D.C. Perng, J.F. Fang, J.W. Chen, Nano-structured ZnSe/CIS heterojunctionsolar cells with ZnSe/ZnO coaxial nanowires. J Electro Chem **158**, H1097–H1101 (2011)
13. T. Yamamoto, S. Kishimoto, S. Iida, Control of valence states for ZnS by triple-codoping method. Phys. B **308–310**, 916–919 (2001)
14. J. Shah, A.E. DiGiovanni, Ac electroluminescence in thin-film ZnSe:Mn. Appl. Phys. Lett. **33**, 995–996 (1978)
15. L. Wang, M. Lu, X.A. Wang, Y.Q. Yu, X.Z. Zhao, P. Lv, H.W. Song, X.W. Zhang, L.B. Luo, C.Y. Wu, Y. Zhang, J.S. Jie, Tuning the p-type conductivity of ZnSe nanowires viasilver doping for rectifying and photovoltaic device applications. J. Mater. Chem. **1**, 1148–1154 (2013)
16. X.S. Fang, Y. Bando, M.Y. Liao, U.K. Gautam, C.Y. Zhi, B. Dierre, B.D. Liu, T.Y. Zhai, T. Sekiguchi, Y. Koide, Single-crystalline ZnS nanobelts as ultraviolet-light sensors. Adv. Mater. **21**, 2034–2039 (2009)
17. Y.Q. Yu, L.B. Luo, M.Z. Wang, B. Wang, L.H. Zeng, C.Y. Wu, J.S. Jie, J.W. Liu, L. Wang, S.H. Yu, Interfacial state induced ultrasensitive ultraviolet light photodetector with resolved flux down to 85 photons per second. Nano Res. (2015). doi:10.1007/s12274-014-0587-8
18. J.J. Hassan, M.A. Mahdi, S.J. Kasim, N.M. Ahmed, H.A. Hansan, Z. Hassan, High sensitivity and fast response and recovery times in a ZnO nanorod array/p-Si self-powered ultraviolet detector. Appl. Phys. Lett. **101**, 261108-1–261108-3 (2012)
19. D. Wu, Y. Jiang, Y.G. Zhuang, J.W. Li, Y.Q. Yu, Y.P. Zhang, Z.F. Zhu, L. Wang, C.Y. Wu, L.B. Luo, J.S. Jie, Device structure-dependent field-effect and photoresponse performances of p-type ZnTe:Sb nanoribbon. J. Mater. Chem. **22**, 6206–6212 (2012)
20. C.W. Liang, S. Roth, Electrical and optical transport of GaAs/Carbon nanotube heterojunctions. Nano Lett. **8**, 1809–1812 (2008)
21. T. Ghosh, M. Dutta, S. Mridha, D. Basak, Effect of Cu doping in the structural, electrical, optical, and optoelectronic properties of sol–gel ZnO thin films. J. Electrochem. Soc. **156**, H285–H289 (2009)
22. D. Wu, Y. Jiang, Y.G. Zhang, Y.Q. Yu, Z.F. Zhu, X.Z. Lan, F.Z. Li, C.Y. Wu, L. Wang, L.B. Luo, Self-powered and fast-speed photodetector based on CdS: Ga nanoribbons/Au Schottky diode. J. Mater. Chem. **22**, 23272–23276 (2012)
23. H. Luo, J.K. Furdyna, The II–VI semiconductor blue–green laser: challenges and solutions. Semicond. Sci. Technol. **10**, 1041 (1995)
24. Y.Q. Yu, J.S. Jie, P. Jiang, L. Wang, C.Y. Wu, Q. Peng, X.W. Zhang, Z. Wang, C. Xie, D. Wu, Y. Jiang, High-gain visible-blind UV photodetectors based on chlorine-doped n-type ZnS nanoribbons with tunable optoelectronic properties. J. Mater. Chem. **21**, 12632–12638 (2011)

25. M.Z. Wang, W.J. Xie, H. Hu, Y.Q. Yu, C.Y. Wu, L. Wang, L.B. Luo, P-type ZnS: N nanowires: low-temperature solvothermal doping and optoelectronic properties. Appl. Phys. Lett. **103**, 213111-1–213111-4 (2013)
26. N. Karar, F. Singh, B.R. Mehta, Structure and photoluminescence studies on ZnS:Mn nanoparticles. J. Appl. Phys. **95**, 656–660 (2004)
27. L.B. Luo, X.B. Yang, F.X. Liang, J.S. Jie, Q. Li, Z.F. Zhu, C.Y. Wu, Y.Q. Yu, L. Wang, Transparent and flexible selenium nanobelt-based visible light photodetector. CrystEngComm **14**, 1942–1947 (2012)
28. Y.Q. Yu, L.B. Luo, Z.F. Zhu, B. Nie, Y.G. Zhang, L.H. Zeng, Y. Zhang, C.Y. Wu, L. Wang, Y. Jiang, High-speed ultraviolet-visible-near infrared photodiodes based on p-ZnS nanoribbon-n-silicon heterojunction. CrystEngComm **15**, 1635–1642 (2013)
29. S.M. Sze, K.K. Ng, J. Wiley, S. Hoboken, *Physics of semiconductor devices*, 3rd edn. (John Wiley & Sons, NJ, 2007)
30. L.H. Zeng, M.Z. Wang, H. Hu, B. Nie, Y.Q. Yu, C.Y. Wu, L. Wang, J.G. Hu, C. Xie, F.X. Liang, L.B. Luo, Germanium/graphene Schottky photodiode. ACS Appl. Mater. Interfaces **5**, 362–9366 (2013)
31. X. Miao, S. Tongay, M.K. Petterson, K. Berke, A.G. Rinzler, B.R. Appleton, A.F. Hebard, High efficiency graphene solar cells by chemical doping. Nano Lett. **12**, 2745–2750 (2012)
32. L.B. Luo, J.J. Chen, M.Z. Wang, H. Hu, C.Y. Wu, Q. Li, L. Wang, J.A. Huang, F.X. Liang, Near infrared light photovoltaic detector based on GaAs nanocones array/monolayer graphene Schottky junction. Adv. Funct. Mater. **24**, 2794–2800 (2014)
33. R. Sharma, A spray drying system for synthesis of rare-earth doped cerium oxide nanoparticles. J. Electron. Dev. **495**, 280–286 (2010)
34. W.F. Jin, Y. Ye, L. Gan, B. Yu, P.C. Wu, Y. Wu, H. Meng, X.F. Guo, L. Dai, Self-powered high performance photodectors based on CdSenanoblet/graphene Schottky junctions. J. Mater. Chem. **22**, 2863–2867 (2012)
35. B. Nie, L.B. Luo, C. Xie, P. Lv, J.S. Jie, M. Feng, F.Z. Li, C.Y. Wu, L. Wang, Y.Q. Yu, S.H. Yu, Monolayer graphene film on ZnO nanorod array for high-performance Schottky junction ultraviolet photodetectors. Small **9**, 2872–2879 (2013)
36. D.S. Tsai, C.A. Lin, W.C. Lien, H.C. Chang, Y.L. Wang, J.H. He, Ultra-high-responsivity broadband detection of Si metal-semiconductor-metal Schottky photodetectors improved by ZnO nanorod arrays. ACS Nano **5**, 7748–7753 (2011)
37. D.C. Kim, B.O. Jung, J.H. Lee, H.K. Cho, J.Y. Lee, J.H. Lee, Dramatically enhanced ultraviolet photosensing mechanism in a n-ZnO nanowires/i-MgO/n-Si structure with highly dense-nanowires and ultrathin MgO layers. Nanotechnology **22**, 265506–265514 (2011)
38. D.B. Li, X.J. Sun, H. Song, Z.M. Li, Y.R. Chen, H. Jiang, G.Q. Miao, Realization of a high-performance GaN UV detector by nanoplasmonic enhancement. Adv. Mater. **24**, 845–849 (2012)
39. T.V. Cuong, H.N. Tien, V.H. Luan, V.H. Pham, J.S. Chung, D.H. Yoo, S.H. Hahn, K.K. Koo, P.A. Kohl, S.H. Hur, E.J. Kim, Solution-processed semitransparent p-n graphene oxide:CNT/ZnO heterojunction diodes for visible-blind UV sensors. Phys. Status Solidi A **208**, 943–946 (2011)
40. X.W. Zhang, J.S. Jie, Z. Wang, C.Y. Wu, L. Wang, Q. Peng, Y.Q. Yu, P. Jiang, C. Xie, Surface induced negative photoconductivity in p-type ZnSe: Bi nanowires and its nano-optoelectronic applications. J. Mater. Chem. **21**, 6736–6741 (2011)
41. S. Panigrahi, A. Bera, D. Basak, Encapsulation of 2-3-nm-sized ZnO quantum dots in a SiO_2 matrix and observation of negative photoconductivity. ACS Appl. Mater. Interfaces **1**, 2408–2411 (2009)
42. S.Y. Wang, W.L. Liu, M. Zhang, Negative photoconductivity and memory effects of germanium nanocrystals embedded in HfO2 dielectric. J. Nanosci. Nanotechnol. **6**, 205–208 (2006)
43. C.Y. Liu, K. Liang, C.C. Chang, Effects of plasmonic coupling and electrical current on persistent photoconductivity of single-layer graphene on pristine and silver nanoparticle coated SiO_2/Si. Opt. Exp. **20**, 22943–22952 (2012)
44. Q. Peng, J.S. Jie, C. Xie, L. Wang, X.W. Zhang, D. Wu, Y.Q. Yu, C.Y. Wu, Z. Wang, P. Jiang, Nano-Schottky barrier diodes based on Sb-doped ZnS nanoribbonswith controlled p-type conductivity. Appl. Phys. Lett. **98**, 123117-1–123117-3 (2011)